Experimental and Numerical Studies on Spherical Roller Bearings Using Multivariable Regression Analysis

R. G. Desavale[1]
Department of Mechanical Engineering,
National Institute of Technology,
Warangal, Andra Pradesh 506 004, India
e-mail: ramdesavale@rediffmail.com

R. Venkatachalam
Department of Mechanical Engineering,
National Institute of Technology,
Warangal, Andra Pradesh 506 004, India
e-mail: chalamrv@yahoo.com

S. P. Chavan
Department of Mechanical Engineering,
Walchand College of Engineering,
Sangli, Maharashtra 416 415, India
e-mail: chavan.walchand@gmail.com

Many industries make wide use of rotor bearing systems such as high speed turbines and generators. However, the vibration of antifriction rotor–bearings is a key factor in reducing the life of the bearings; thus significantly influencing the performance and working life of the whole power plant. In earlier research on the vibration characteristics of high speed rotor–bearing systems, such as in induced draft (ID) fans, an application used in sugar cane factories, the supporting antifriction bearings were simplified as a particle on a shaft with radial stiffness and damping coefficient. However, such simplification neglects the effects of the bearing structure on the vibration performance of the rotor–bearing system. This paper demonstrates the benefits of a more holistic approach and establishes a numerical model of the stiffness of the spherical roller bearing through Buckingham's π theorem (BPT). On the basis of this model, we argue for the benefits of a new dimensional analysis (DA) technique for rotor–bearing systems. Our new DA also considers the influences of the bearing structure parameters on the vibration of rotor–bearing systems. We demonstrate the effectiveness of our approach by conducting a comparative BPT study using an ID fan, a rotor–bearing system in use in sugar cane factories. We first analyzed an ID fan using the simplified model to obtain the defect frequencies and vibration amplitude responses of the ID fan system. Subsequently the same ID fan rotor was also analyzed using our new multivariable regression analysis (MVRA) approach to verify the validity of our new and holistic BPT. The results indicate that the new method we propose in this paper for the calculation of vibration characteristics of a high speed rotor–bearing (ID fan) is credible and will save time and costs by the accurate detection of imminent bearing failure. [DOI: 10.1115/1.4026433]

Keywords: multivariable regression analysis, double row spherical roller bearing, ID fan, BPT, high speed rotor–bearings

1 Introduction

Systems with high speed rotors supported by double row spherical roller bearings are widely used in many industries [1]. In application, these systems often face many different problems which influence the efficient working process of the plant, such as sugar factories, which use ID fans. One of the most common problems of these systems is vibration. The vibration calculation of rotor–bearings is a focus in the many engineering fields. In sugar factory applications, the vibration in ID fans mainly originates from the wavering of the ID fan hammers and rotor–bearing system [2,3], with the rotor–bearing system as the crucial source. The most important vibration parameters of the ID fan rotor include load and speed, unbalanced response, etc. To obtain these parameters, the stiffness and damping of the supporting rolling element bearing should first be considered in order to establish the governing equations of the whole system by using BPT. On this basis, the dynamic characteristics of an ID fan rotor system can be revealed and the vibration parameters can be obtained.

Previous researchers who focused on the vibration of radial ball bearings were Rahnejat and Gohar [4]. They built a deep groove ball bearing model including an extrapolated equation that considered the effect of squeeze film. They suggested that the number of balls, applied load, and radial internal clearance affects the limit cycle frequency and amplitude of the ball bearing. Even in the presence of elastohydrodynamic lubricating film between balls and the raceways, a peak of the ball passage frequency (BPF) appears in the spectrum [5].

Tomovic et al. [6] studied the vibration response of rigid rotors in unloaded rolling element bearings. By the application of the defined model, they performed a parametric analysis of the effect of internal radial clearance value and the influence of the number of rolling elements on rigid rotor vibrations in unloaded rolling element bearings. They concluded that the BPF linearly increases with the increase of the number of rolling elements. This increase is more pronounced with lower values of ratio between diameter of rolling elements and cage pitch diameter. With the increase of the internal radial clearance, the value of amplitude increases linearly. The increase gets much bigger as the total number of rolling elements decreases.

Patil et al. [7] developed a theoretical model to predict the effect of localized defect on vibrations associated with ball bearings. The contacts between the ball and the races are considered as nonlinear springs. The contact force is calculated using the Hertzian contact deformation theory. The results are presented in the forms of time and frequency domains. Experiments were carried out on 6305 deep groove ball bearings. They concluded that the amplitude level of vibrations in case of outer race defects is more than that for inner race and ball defects. It was also predicted from the model that the amplitude of vibration increases with the

[1]Corresponding author.

Contributed by the Design Engineering Division of ASME for publication in the JOURNAL OF VIBRATION AND ACOUSTICS. Manuscript received April 13, 2013; final manuscript received December 11, 2013; published online February 5, 2014. Assoc. Editor: Mary Kasarda.

increase in the defect size and it is observed through experimentation.

Kankar et al. [8] investigated the fault diagnosis of ball bearings using machine learning methods. This study focused on the fault diagnosis of ball bearings using an artificial neural network (ANN) and support vector machine (SVM). The specific defects are considered as cracks in outer and inner races with rough surface and corrosion pitting in balls. Kankar et al. [8] carried out a comparative experimental study of the effectiveness of ANN and SVM. The results show that the machine learning algorithms mentioned above can be used for automated diagnosis of bearing faults. It was concluded that the accuracy of SVM is better than of ANN. Both the machine learning methods give less accuracy in correctly predicting the bearing condition with combined bearing component faults, though results obtained from SVM are slightly better than ANN. This demonstrates that the application of defect diagnosis for condition-based maintenance prevents catastrophic failure and reduces operating cost.

From the above literatures, it can be seen that in the past research articles have highlighted the different techniques used for the detection of faults [9]. The key challenge for fault diagnosis is the improvement of the accuracy of diagnostics based on a given amount of information. While previous research indicates that much work has been done on ball bearings, identification of the wider combination of defects in rolling bearing elements has been limited. Our literature research indicates that only very little work has been done on spherical roller bearings to date. In response, this paper presents a new analytical model for calculating overall vibration, defect frequencies, stiffness, and damping of the spherical roller bearing, and provides a numerical model for calculating defects in high speed rotor–bearing systems. An actual ID fan was analyzed with the new BPT to show that the bearing structure significantly affects the vibration characteristics of a rotor–bearing system. The rotor was also analyzed using MVRA and ANN.

2 Formulation of Dimensional Analysis

2.1 Modeling Spherical Roller Bearings. A real rotor–bearing system is generally very complicated and difficult to model. The functional dependence of vibration amplitude on the parameters can be estimated by performing a DA based on the BPT. In this work, an analytical model is proposed for estimating the vibration amplitude in antifriction bearings by using the concepts of DA and including the parameters below. Knowing the governing parameters of the physical problem and by using the concepts of BPT, relationships are obtained between the different parameters involved [10–22]. The first task is to identify a relevant set of bearing variables. The set should be "complete," such that none of the independent variables can be derived from others, while the dependent variables can be so derived [23]. The independent variables relate to bearing geometry, operating conditions, and the properties of all materials. In this study the dependent variables are load and speed. A suitable set of variables is given in Table 1. A mass–length–time (MLT) units' reference set is used. According to the numerical model for antifriction bearings proposed in this paper, the functional relationship is the following. The vibration amplitude (A) can be given by an equation of the form (2). Where F is an unknown function, assuming that this function is in the form of a product of powers. The number of dimensionless products in a complete set is equal to the total number of variables minus the maximum number of these variables that will not form a dimensionless product. Therefore, the number of the independent group m is, according to BPT [16,23], the number of independent dimensionless π products is

$$(36 \text{ variables}) - (3 \text{ reference dimensions}) = 33\pi - \text{terms}$$

Table 1 Parameters for modeling spherical roller bearings

Parameters	Symbols	SI units	Dimensions
Geometric parameters			
Bore diameter	D	m	L
Roller diameter	d_b	m	L
Inner race diameter	d_i	m	L
Outer race diameter	d_o	m	L
Pitch diameter	d_m	m	L
No. of rollers	Z	—	—
Radial clearance	C_r	m	L
Inner groove diameter	d_{gi}	m	L
Outer groove diameter	d_{go}	m	L
Initial position of the defect	θi	—	—
Height of defect (size)	H_d	m	L
Length of roller	L	m	L
Bearing width	B	m	L
No. of defects	n_d	—	—
Properties of double row spherical roller bearing			
Mass of rotor	m_r	kg	M_r
Mass of the inner race	m_i	kg	M_i
Mass of the outer race	m_o	kg	M_o
Mass of the roller	m_b	kg	M_b
Spring constant	K	N/m	MT^{-2}
Damping	C	N S/m	MT^{-1}
Properties of lubricant			
Lubricant viscosity	H	N s/m^2	$ML^{-1}T^{-1}$
Impact parameters			
Speed of shaft	N	rpm	T^{-1}
Resisting torque (frictional)	T	N m	ML^2T^{-2}
Radial load	W	N	MLT^{-2}
Material parameters			
Young's modulus	E	N/m^2	$ML^{-1}T^{-2}$
Density of bearing material	ρ	kg/m^3	ML^{-3}
Poisson's ratio's	ν	—	$M^0L^0T^0 = 1$
Coefficient of friction	μ	—	$M^0L^0T^0 = 1$
Response parameters			
Amplitude	A	mm	L
Deflection	δ	mm	L
Acceleration	a	m/s^2	LT^{-2}
Stresses	S	N/m^2	$ML^{-1}T^{-2}$
Cage frequency	f_c	Hz	T^{-1}
Roller spinning frequency	f_b	Hz	T^{-1}
Inner race defect frequency	f_{id}	Hz	T^{-1}
Outer race defect frequency	f_{od}	Hz	T^{-1}
Roller defect frequency	f_{bd}	Hz	T^{-1}

It may be assumed that the vibration amplitude depends on the speed, radial load, and density of the material, lubricant viscosity, stiffness and damping, and temperature. In antifriction bearings, speed and load have a significant role to play in changing the vibration amplitude. The dimensions of all these quantities are reported in the M, L, T, θ system as shown in Table 1. All the above variables considered for the problem are assembled using BPT in a number of dimensional products (π_i) as follows [23]. That is, we have

$$F(\pi_1, \pi_2, \pi_3, \pi_4, \pi_5, \pi_6, \ldots, \pi_{m-n}) = 0 \quad (1)$$

In the lower part of Table 2, according to the procedure, the formulation of the dimensionless numbers is obtained. In this regard, as we anticipated above, the BPT does not give any hint concerning the form of the new equation, or the best dimensionless set to be developed out of the starting dimensional variables. This will allow a better experimental control, and simplify the search of the functional form of the dimensionless equation.

Table 2 Prediction and design equations for dynamic response of spherical roller bearings

Sr.	Basic π relation	
Prediction equations		
1	Π_1	$\frac{a_o}{D}$
2	Π_2	$\frac{d_b}{D}$
3	Π_3	$\frac{d_i}{D}$
4	Π_4	$\frac{d_o}{D}$
5	Π_5	$\frac{d_m}{D}$
6	Π_6	Z
7	Π_7	$\frac{C_r}{D}$
8	Π_8	$\frac{d_{gi}}{D}$
9	Π_9	$\frac{d_{go}}{D}$
10	Π_{10}	θ_i
11	Π_{11}	$\frac{H_d}{D}$
12	Π_{12}	$\frac{L}{D}$
13	Π_{13}	$\frac{B}{D}$
14	Π_{14}	n_d
Design equations		
1	Π_{15}	$\frac{KD}{W}$
2	Π_{16}	$\frac{CND}{W}$
3	Π_{17}	$\frac{\eta D^2 N}{W}$
4	Π_{18}	$\frac{T}{WD}$
5	Π_{19}	$\frac{m_r D N^2}{W}$
6	Π_{20}	$\frac{m_i D N^2}{W}$
7	Π_{21}	$\frac{m_o D N^2}{W}$
8	Π_{22}	$\frac{m_b D N^2}{W}$
9	Π_{23}	$\frac{S D^2}{W}$
10	Π_{24}	$\frac{\delta}{W}$
11	Π_{25}	$\frac{f_c}{N}$
12	Π_{26}	$\frac{f_b}{N}$
13	Π_{27}	$\frac{f_{id}}{N}$
14	Π_{28}	$\frac{f_{od}}{N}$
15	Π_{29}	$\frac{f_{bd}}{N}$
16	Π_{30}	$\frac{E D^2}{W}$
17	Π_{31}	$\frac{\rho D^4 N^2}{W}$
18	Π_{32}	υ
19	Π_{33}	μ

The DA is a convenient tool to perform studies and understand the effects of various important parameters involved. The fact that no attempt has been observed on applying DA for rolling element bearings indicates that this forms a gap in the research work relating to the antifriction bearings

$$\begin{aligned}\text{Amplitude}(A) = F(&D, d_b, d_i, d_o, d_m, Z, C_r, d_{gi}, d_{go}, \theta_i, H_d,\\ &l_r, B, n_d, N_s, W, K, C, \eta, T_f, m_r, m_i, m_o, S, \delta, E, \rho,\\ &\nu, f_c, f_b, f_{id}, f_{od}, f_{bd}, a)\end{aligned} \tag{2}$$

2.2 Reduction Dimensionless Forms. The observation that a dimensionally homogeneous equation among several variables can be reduced to an equation among a smaller number of dimensionless variables is principally due to Rayleigh and Buckingham. For each of the problems, it can be shown that the two Π terms combine to form the high-level dimensionless variables as follows:

$$\pi_a = \frac{\pi_2}{\pi_5} = \frac{d_b}{D}, \quad \frac{D}{d_m} = \frac{d_b}{d_m} \tag{3}$$

$$\pi_b = \frac{\pi_3}{\pi_4} = \frac{d_i}{D}, \quad \frac{D}{d_o} = \frac{d_i}{d_o} \tag{4}$$

$$\pi_c = \frac{\pi_7}{\pi_{12}} = \frac{C_r}{D}, \quad \frac{D}{I_r} = \frac{C_r}{I_r} \tag{5}$$

$$\pi_d = \frac{\pi_{11}}{\pi_{13}} = \frac{H_d}{D}, \quad \frac{D}{B} = \frac{H_d}{B} \tag{6}$$

$$\pi_e = \frac{\pi_9}{\pi_8} = \frac{d_{go}}{D}, \quad \frac{D}{d_{gi}} = \frac{d_{go}}{d_{gi}} \tag{7}$$

$$\pi_f = \frac{\pi_{19}}{\pi_{22}} = \frac{m_r D N^2}{W}, \quad \frac{W}{m_b D N^2} = \frac{m_r}{m_b} \tag{8}$$

$$\pi_g = \frac{\pi_{21}}{\pi_{20}} = \frac{m_o D N^2}{W}, \quad \frac{W}{m_i D N^2} = \frac{m_o}{m_i} \tag{9}$$

$$\pi_h = \frac{\pi_{15}}{\pi_{16}} = \frac{KD}{W}, \quad \frac{W}{CND} = \frac{K}{CN} \tag{10}$$

$$\pi_i = \frac{\pi_{17}}{\pi_{18}} = \frac{\eta D^2 N}{W}, \quad \frac{WD}{T} = \frac{\eta D^3 N}{T} \tag{11}$$

$$\pi_j = \frac{\pi_{23}}{\pi_{24}} = \frac{S D^2}{W}, \quad \frac{D}{\delta} = \frac{S D^3}{\delta W} \tag{12}$$

$$\pi_k = \frac{\pi_{30}}{\pi_{31}} = \frac{E D^2}{W}, \quad \frac{D}{\rho D^4 N^2} = \frac{E}{\rho D^2 N^2} \tag{13}$$

$$\pi_l = \pi_h, \quad \pi_i = \frac{K}{CN}, \quad \frac{\eta D^3 N}{T} = \frac{\mathrm{K}\eta D^3}{CT} \tag{14}$$

$$\pi_m = \frac{\pi_k}{\pi_j} = \frac{\rho D^2 N^2}{E}, \quad \frac{\delta W}{S D^3} = \frac{\rho D^2 \delta W}{E S D} \tag{15}$$

$$\pi_n = \frac{\pi_{26}}{\pi_{25}} = \frac{f_b}{f_c} \tag{16}$$

$$\text{Constant} = \beta = \left(\pi_\mathrm{a}, \pi_\mathrm{b}, \pi_\mathrm{c}, \pi_\mathrm{d}, \pi_\mathrm{e}, \pi_\mathrm{f}, \pi_\mathrm{g}, \mathrm{Z}, \theta\mathrm{i}, \mathrm{n_d}, \upsilon, \mu\right) \tag{17}$$

$$\begin{aligned}\text{Constant} = \beta &= (Z, \theta_i, n_d, \upsilon, \mu), \left(\frac{d_b}{d_m}, \frac{d_i}{d_o}, \frac{d_{go}}{d_{gi}}\right), \left(\frac{C_r}{L}, \frac{H_d}{B}\right), \left(\frac{m_r}{m_b}, \frac{m_o}{m_i}\right)\end{aligned} \tag{18}$$

Substituting for various dimensionless groups, equations may be rewritten as in Eqs. (19)–(24):

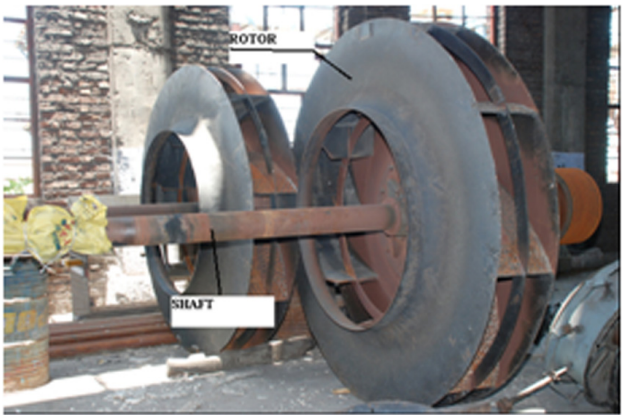

Fig. 1 Photographic views of ID fan rotor–bearing

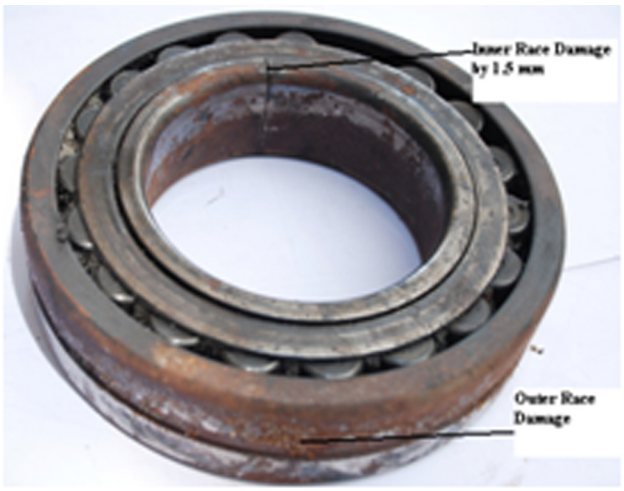

Fig. 2 Inner race and cage with defects

$$\frac{a_o}{D} = F\left(\beta, \frac{1}{Z}, n_d, \frac{C_r}{L}, \frac{H_d}{B}, \frac{K\eta D^3}{CT}, \frac{\rho N^2 \delta W}{ESD}, \frac{f_b}{f_c}, \frac{f_{id}}{N}, \frac{f_{od}}{N}, \frac{f_{bd}}{N}\right) \quad (19)$$

$$a = F\left(\beta, \frac{1}{Z}, \frac{a_0}{D}, n_d, \frac{C_r}{L}, \frac{H_d}{B}, \frac{K\eta D^3}{CT}, \frac{\rho N^2 \delta W}{ESD}, \frac{f_b}{f_c}, \frac{f_{id}}{N}, \frac{f_{od}}{N}, \frac{f_{bd}}{N}\right) \quad (20)$$

$$\frac{f_b}{f_c} = F\left(\beta, \frac{1}{Z}, \frac{a_0}{D}, n_d, \frac{C_r}{L}, \frac{H_d}{B}, \frac{K\eta D^3}{CN}, \frac{\rho N^2 \delta W}{ESD}, a, \frac{f_{id}}{N}, \frac{f_{od}}{N}, \frac{f_{bd}}{N}\right) \quad (21)$$

$$\frac{f_{id}}{N_s} = F\left(\beta, \frac{1}{Z}, \frac{a_0}{D}, n_d, \frac{C_r}{L}, \frac{H_d}{B}, \frac{K\eta D^3}{CN}, \frac{\rho N^2 \delta W}{ESD}, \frac{f_b}{f_c}, a, \frac{f_{od}}{N}, \frac{f_{bd}}{N}\right) \quad (22)$$

$$\frac{f_{od}}{N_s} = F\left(\beta, \frac{1}{Z}, \frac{a_0}{D}, n_d, \frac{C_r}{L}, \frac{H_d}{B}, \frac{K\eta D^3}{CT}, \frac{\rho N^2 \delta W}{ESD}, \frac{f_b}{f_c}, \frac{f_{id}}{N}, a, \frac{f_{bd}}{N}\right) \quad (23)$$

$$\frac{f_{bd}}{N_s} = F\left(\beta, \frac{1}{Z}, \frac{a_0}{D}, n_d, \frac{C_r}{L}, \frac{H_d}{B}, \frac{K\eta D^3}{CT}, \frac{\rho N^2 \delta W}{ESD}, \frac{f_b}{f_c}, \frac{f_{id}}{N}, \frac{f_{od}}{N}, a\right) \quad (24)$$

Equations (19)–(24) show the model for predictions and calculating defects, vibration amplitude, acceleration, cage frequency, roller spinning frequency, inner race defect frequency, outer race defect frequency, and roller defect frequency (Figs. 2 and 3). Finally, a functional relationship is proposed for the amplitude of vibration in terms of dimensionless parameters. The dependence is to be investigated through experimental study.

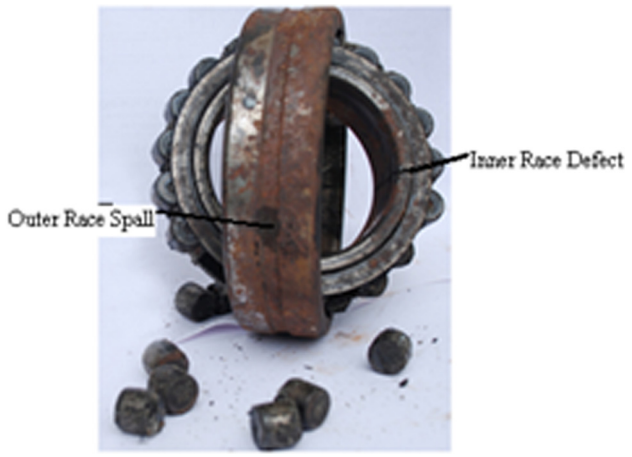

Fig. 3 Outer race and inner race with defects

3 Experimental Details

3.1 Experimental Procedure. The experimental setup used for this study is shown in Fig. 1. It is consists of a shaft supported on two bearings and driven by a constant speed turbine. The test bearing, a double roller taper, spherical roller bearing 23,222 CCK/W33/C3-SKF Sweden, is placed on the nondrive end of the shaft and a double-row self-aligning spherical roller bearing is placed on the drive end side. The ID fan rotor arrangement is placed between these two bearings as shown in Fig. 1. A piezoelectric accelerometer with a sensitivity of 100 mV/g is used to measure the vibrations. It is mounted on the housing of the test bearing. The accelerometer is connected to the fast Fourier transform (FFT) analyzer, the output of which is connected to a computer, and displays the time domain signal. The experiments have been performed on separate test bearings having defects of sizes 1.5 mm, 2 mm, and on an outer race, inner race, and rollers of a damaged bearing; separately, Figs. 2 and 3 shows different faults. Then, data are collected for different fault conditions. A variety of faults are simulated on the rig at 1000 and 4400 rpm. The following faults are introduced in the bearing:

- outer race with defect, Fig. 2
- inner race with defect, Fig. 3

Vibration responses for all cases are presented in FFT form. MVRA is used to find the effects of various localized bearing component faults on vibration responses and interactions between faults. In order to perform MVRA to determine the combination of defects, DOE is used with a total of 27 trial runs. Table 3 shows parameters used for DOE with their minimum and maximum levels.

4 Experimental Designs Analysis of Variance

4.1 Analysis of Variance (ANOVA). ANOVA gives a summary of the main effects and interactions, of regression coefficients, and p value (Fig. 4). The p value in the ANOVA analysis helps to determine which effects (factors and interactions) are statistically significant. p values are often used in hypothesis tests where you either accept or reject a null hypothesis. The p value represents the probability of making a type-I error or rejecting the null hypothesis when it is true. The smaller the p value, the smaller is the probability that you would be making a mistake by rejecting the null hypothesis. The cutoff value often used is 0.0500, i.e., reject the null hypothesis when the p value is less

Table 3 Levels of the variables of the experimental design

Design variable	Design parameter	Levels		
		Level 1	Level 2	Level 3
A Inner race defect	R_i	0	1	2
B Outer race defect	R_o	0	1	2
C Roller defect	R_r	0	1	2
D Speed	N_s	1000	2500	5000
E Defect size	d_B	0	1	2
F Load	W	0	1	2
G Number of rollers	Z	8	13	17
H Number of defects	d_N	0	1	2
I Radial clearance	Cr	0	0.02	0.08
J Stiffness	K	0	2.5×10^8	4.0×10^8
K Damping	C	100	200	300
L Unbalance	U_b	100	200	300

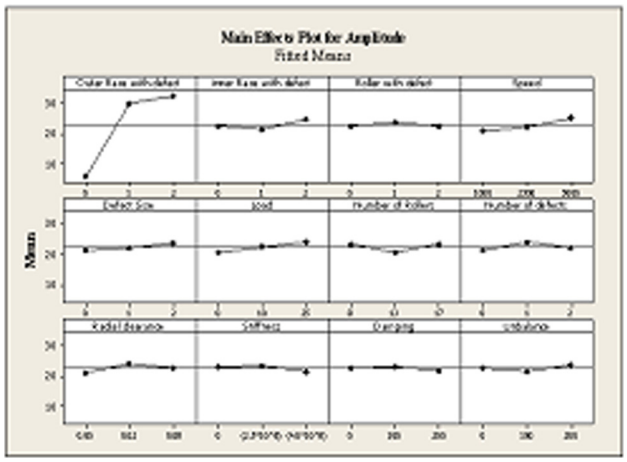

Fig. 4 Main effect of plots (vibration amplitude)

than 0.0500. It is common to declare a result significant if the p value is less than 0.0500 [17].

4.2 Multivariable Regression Modeling. MVRA refers to techniques for the modeling and analysis of numerical data consisting of values of a dependent variable and of one or more independent variables. The dependent variable in the multivariable regression equation is modeled as a function of the independent variables, corresponding parameters, and an error term. The error term is treated as a random variable and represents unexplained variation in the dependent variable. Parameters are estimated to give a "best fit" of the data. Most commonly the best fit is evaluated by using the least squares method, but other criteria have also been used. The linear model under the multivariate setup is

$$y_i = b_0 + b_1X_1 + b_2X_2 + b_3X_3 + \cdots + b_pX_p + e_i \qquad (25)$$

where y is a dependent variable, $X_1, X_2,\ldots,X_p$ are independent variables, and n observations on each of the p independent variables are available. The regression coefficients associated with X_1, $X_2,\ldots, X_p$ are $\beta_1, \beta_2,\ldots, \beta_p$, respectively, and β_0 is the involved intercept term in the model. The random error component e_i takes care of all the random factors affecting y not included in the model and is assumed to be identically and independently distributed following a normal distribution with mean and constant variance σ^2. The MVRA is done in terms of the fitted surface. Once a regression analysis model is obtained, statistical analysis techniques, such as ANOVA, can be used to check the fitness of the model. Regression equations are found out using software for statistical analysis called MINITAB 16. The regression equation helps to get the relation between different response variables (amplitude and frequency) and the input parameters (speed, load, and diameter). The software required the input conditions and the observations of the experiments and developed the regression equations for each desired output. Based on the experimental runs, following regression equations are obtained.

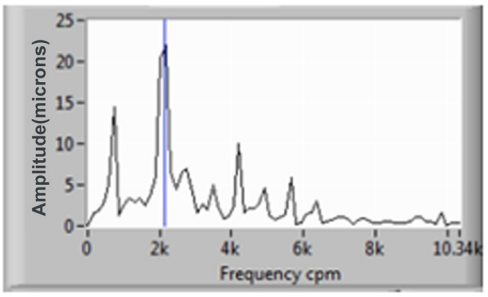

Fig. 5 Response plot for rotor speed 1000 rpm (H)

These 12 factors are selected with three levels. The upper and lower levels of each factor are defined in Table 3. The reference value for healthy and defective bearings are taken as 0 and 1, 2 respectively, where value 0 indicates absence of defect and values 1 and 2 indicate that defect is present in bearing components. DOE considers factors with two levels and eight trial runs, as listed in Table 3.

5 Discussions of the Results

The equations of motion (19) has been solved by the DA method to obtain the displacement and vibration amplitude, and defect frequencies of the antifriction bearings. For the trials 1–27 (as shown in Table 3), the response plots have been shown in the form of frequency spectra obtained from the experimental data based mathematical model and experimental analysis, as shown in Figs. 5–13, respectively. Figure 5 shows the response plots for the minimum level of localized defects of bearing components with the ID fan rotor speed at 1000 rpm. For this trial, peak amplitude of vibration excitation appears at multiples of frequency spectra. The mathematical model equation (19) confirms the multiple peaks of excitation of FFT and shows the periodicity of the system. In the presence of defects on the outer race at 2500 rpm of ID fan rotor speed, the peak amplitude of vibration appears in the spectrum at roller passage frequency and its multiples, as shown in Fig. 12. The broad band frequency spectrum that appears around the peak of excitation shows that the system loses its periodicity, which can also be confirmed by Eq. (19). Figure 13 shows the response with a defect on the inner race with 2500 rpm of ID fan rotor speed. For this trial, the peak amplitude of vibration responses appears at wave passage frequencies and this shows the onset of a damaged condition. The experiment then increased the ID fan rotor speed to 5000 rpm, i.e., at maximum load level. We found that when the system operates with healthy bearings at a rotor speed of 5000 rpm, the second order subharmonic nature is observed with peak amplitude of vibration and appears at a certain harmonics in the frequency spectrum, as shown in Figs. 10 and 11.

The MINITAB statistical package was used to analyze the experimental data and response parameters. The significant terms in the model were found by ANOVA at 5% level of significance (95% confidence level). The regression coefficients are obtained using the coded units. Table 4 shows the regression coefficients and p value.

Table 5 shows that for trials 1–27 the peak amplitude of vibration appears in the spectrum for horizontal acceleration responses

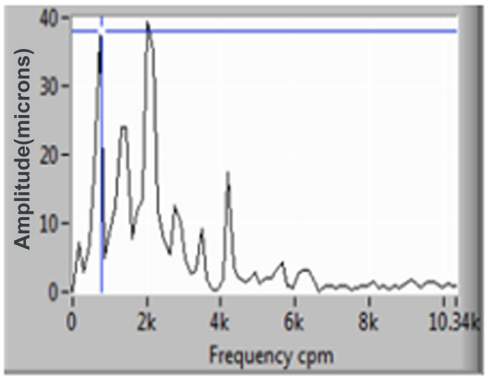

Fig. 6 Response plot for rotor speed 2500 rpm (H)

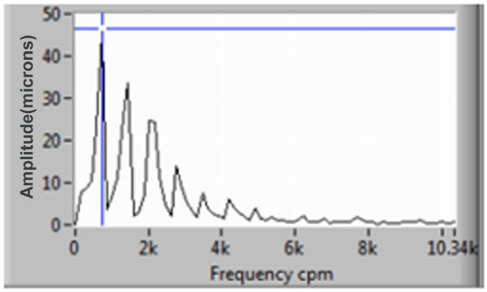

Fig. 7 Response plot for rotor speed 5000 rpm (H)

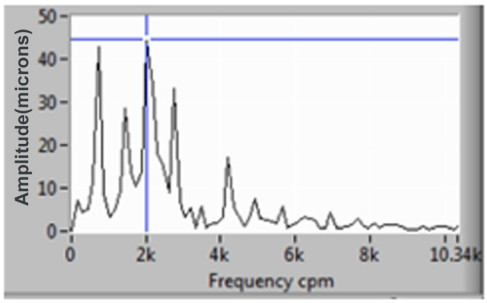

Fig. 8 Response plot for rotor speed 5000 rpm (outer race defect)

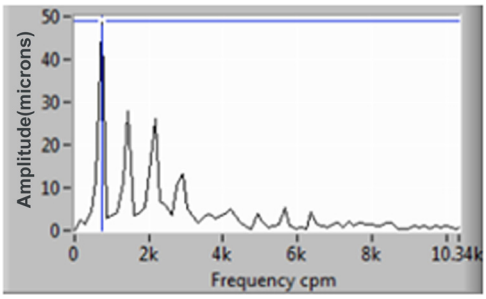

Fig. 9 Response plot for rotor speed 5000 rpm (inner race defect)

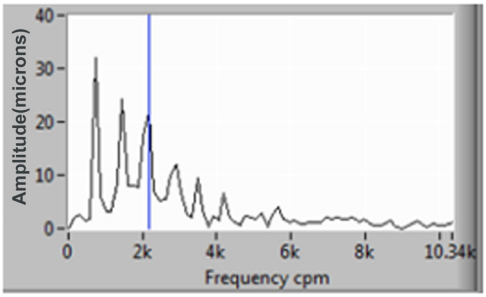

Fig. 10 Response plot for rotor speed 2500 rpm (outer race defect)

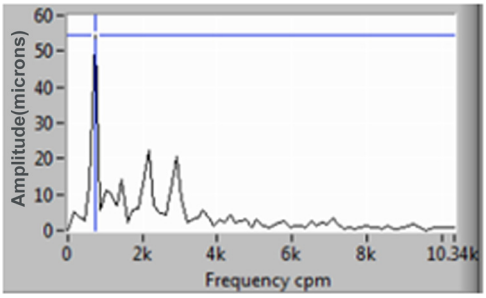

Fig. 11 Response plot for rotor speed 2500 rpm (inner race defect)

and for vertical acceleration responses. Through the experiments, the polynomials $f(x)$ are approximated by the design parameters/variables. The final functions of the multivariable regression analysis model are listed below. The second-degree polynomial for horizontal acceleration responses are

$$\begin{aligned}&\text{Vibration acceleration}\\&= 1.57 + 13.5\,\text{outer race with defect} + 1.32\,\text{inner race with defect}\\&\quad + 0.11\,\text{roller with defect} + 0.00106\,\text{speed} + 1.30\,\text{defect size}\\&\quad + 0.141\,\text{load} - 0.041\,\text{number of rollers} + 0.32\,\text{number of defects}\\&\quad + 10.3\,\text{radial clearance} - 0.0041\,\text{damping} + 0.0060\,\text{unbalance}\end{aligned} \tag{26}$$

The performance prediction of vibration amplitude in horizontal and vertical acceleration responses has been shown in Fig. 14. The actual and predicted values of responses in both directions are very close and verify the fitness of polynomials for the responses obtained. In order to verify whether the obtained polynomials are valuable or not, we performed variance analysis and F-ratio tests on them. Table 6 shows the ANOVA tables for horizontal displacement. The model F value of 51.16 implies that the model is significant. The p values less than 0.0500 indicate that model terms are significant. In this case, A, B, D, E, and H are significant model terms. The values greater than 0.1000 indicates the model terms are not significant. ANOVA for vertical displacement is shown in Table 3. F value of 51.160 implies that the model is significant. In this case, A, B, D, E, and H are significant model terms.

The ANOVA tests of both polynomials show that they are valuable for the corresponding problems [17]. They can be used to analyze the relation between factors and their corresponding responses. After testing the polynomials using ANOVA, MVRA of horizontal and vertical acceleration responses are developed. The response surface in Fig. 17 shows the interaction effect of an outer race defect and an inner race defect on horizontal responses. The presence of a defect in inner and outer races increases the amplitude of vibration.

The response surfaces in Figs. 15 and 16 show the interaction effects of roller defects with outer race and inner race defects on horizontal responses, respectively. With outer race defects the amplitude of vibration increases, but decreases with inner race defects in the presence of roller defects. Roller defects have very

Table 4 Bearing parameters

Parameters	Values
Outer race diameter	200 mm
Inner race diameter	110 mm
Roller diameter	15 mm
Number of rollers	19/19
Contact angle	0 deg
Radial clearance	7 μm
Defect on inner race roller crack	2 mm
Defect on outer race	2 mm
Mass	9.85 kg
Width	69.8 mm

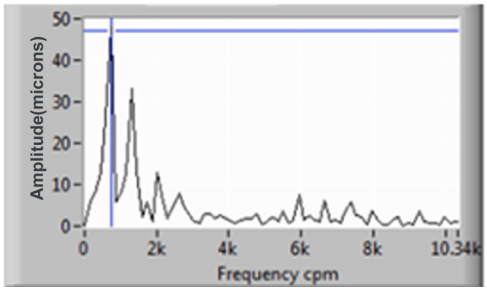

Fig. 12 Response plot for rotor speed 5000 rpm (roller defect)

little effect on the horizontal amplitude of vibration. Rotor speed has considerable effect on the horizontal amplitude of vibration. In the presence of outer race defects in bearings, the horizontal amplitude of vibration increases more at a rotor speed of 5000 rpm compared to a rotor speed of 1000 rpm, as shown in Fig. 15. With inner race bearing defects and at a rotor speed of 5000 rpm, the catastrophic stage of bearing failure started and due to "self-peening" of the bearing, the amplitude of vibration decreased, as shown in Fig. 15.

6 Artificial Neural Networks

6.1 Modeling of Bearings. In recent times, the application of artificial intelligence techniques is increasing tremendously in almost all engineering areas. Modeling and optimization are necessary for the understanding and control of any process. Precise control is a prerequisite to achieve improved quality and productivity. Artificial neural network plays an important role in predicting the linear and nonlinear problems in different fields of engineering. Many attempts have been made of the multilayer Perceptron [18,19].

A multilayer Perceptron trained with the backpropagation algorithm may be viewed as a practical way of performing a linear input–output mapping of a general nature (Fig. 17). Backpropagation neural networks are usually referred to as a feed forwarded, multilayered network with a number of hidden layers trained with a gradient descent technique. This algorithm is based on the error correction learning rule. Basically, the error backpropagation process consists of two passes through the different layers of the network: a forward pass and a backward pass. In the forward pass, an activity pattern (input vector) is applied to the sensory nodes of the network, and its effect propagates through the network layer by layer. Finally, a set of outputs is produced as the actual response of the network. During the backward pass, all synaptic weights are adjusted in accordance with the error correction rule. Specifically, the actual response of the network is subtracted from the desired (target) response to produce an error signal. The synaptic weights are adjusted so as to make the actual response of the network move closer to the desired network.

6.2 Simulation Procedure. The objective of the simulation was to first have the system learn the appropriate mappings between input and output variables by observing the training samples. The trained system was then used to determine the input conditions that maximize vibration amplitude (A) subject to certain constraints. The three layer backpropagation with four inputs, two outputs, and nine hidden nodes was employed for the neural network. The network was trained using 54 samples that span the allowable ranges of input variables. The inputs were defects (n_d), load (W), number of rollers (Z), speed (N_S), and outputs were amplitude (A) and frequencies (f_{bd}). A random generator was used to initialize the values of the learning parameter. In order to decide the structure of the neural network, the rate of error convergence was checked by changing the number of hidden layers and also by adjusting the learning rate and momentum rate. As a result, a neural network with nine neurons in the hidden layer was adopted for storing knowledge in the form of weights between neurons. A crucial problem in backpropagation is its generalization ability. There is no certainty that the network successfully trained on the given samples provides desired input/output associations for the untrained pattern as well. As the number of neurons increases the approximation for weight increases and as a result we get an overfitted network model where a lesser number of neurons in the hidden layer are not capable of giving the desired result, therefore it is necessary for any neural network that the number of neurons in the hidden layer should be appropriate. It is seen that for 85% of the cases the single neuron is enough and for the other 15% of the cases two neurons are needed to train any neural network to get a good result.

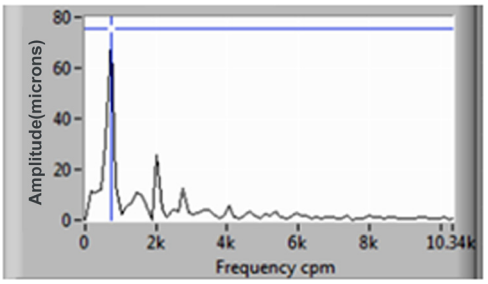

Fig. 13 Response plot for rotor speed 2500 rpm (inner race defect)

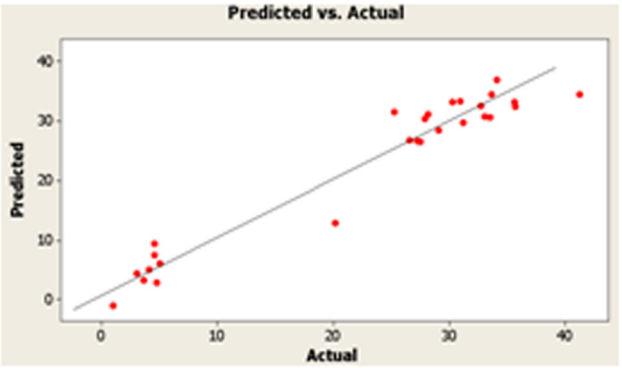

Fig. 14 The performance prediction: Horizontal acceleration response

6.3 Validation of Model. The measurements are collected at different points, all in machine bearing housings, to detect various types of defects as shown in Fig. 1. Also, vibrations are measured along axial, horizontal, and vertical directions. Vibration signals are collected by means of a closed, proprietary vibration analyzer equipped with a sensor in the frequency domain and vibration signal techniques were applied within the system. There are a number of factors that contribute to the complexity of the bearing

Table 5 Orthogonal array L27 of Taguchi method for vibration amplitude without damping

Ex. No.	1	2	3	4	5	6	7	8	9	10	11	12	Response amplitude peak (g)
1	0	0	0	1000	0	0	8	0	0.00	0	0	0	0.971
2	0	0	0	1000	1	10	13	1	0.02	2.5×10^8	100	100	3.651
3	0	0	0	1000	2	25	17	2	0.08	4.0×10^8	200	200	4.086
4	0	1	1	2500	0	0	8	1	0.02	2.5×10^8	200	200	4.789
5	0	1	1	2500	1	10	13	2	0.08	4.0×10^8	0	0	3.076
6	0	1	1	2500	2	25	17	0	0.00	0	100	100	4.560
7	0	2	2	5000	0	0	8	2	0.08	4.0×10^8	100	100	5.010
8	0	2	2	5000	1	10	13	0	0.00	0	200	200	4.566
9	0	2	2	5000	2	25	17	1	0.02	2.5×10^8	0	0	20.198
10	1	0	1	5000	0	10	17	0	0.02	4.0×10^8	0	100	29.094
11	1	0	1	5000	1	25	8	1	0.08	0	100	200	41.229
12	1	0	1	5000	2	0	13	2	0.00	2.5×10^8	200	0	27.871
13	1	1	2	1000	0	10	17	1	0.08	0	200	0	26.560
14	1	1	2	1000	1	25	8	2	0.00	2.5×10^8	0	100	25.230
15	1	1	2	1000	2	0	13	0	0.02	4.0×10^8	100	200	27.230
16	1	2	0	2500	0	10	17	2	0.00	2.5×10^8	100	200	33.526
17	1	2	0	2500	1	25	8	0	0.02	4.0×10^8	200	0	31.210
18	1	2	0	2500	2	0	13	1	0.08	0	0	100	28.130
19	2	0	2	2500	0	25	13	0	0.08	2.5×10^8	0	200	30.282
20	2	0	2	2500	1	0	17	1	0.00	4.0×10^8	100	0	27.508
21	2	0	2	2500	2	10	8	2	0.02	0	200	100	35.674
22	2	1	0	5000	0	25	13	1	0.00	4.0×10^8	200	100	30.970
23	2	1	0	5000	1	0	17	2	0.02	0	0	200	33.651
24	2	1	0	5000	2	10	8	0	0.08	2.5×10^8	100	0	34.086
25	2	2	1	1000	0	25	13	2	0.02	0	100	0	32.748
26	2	2	1	1000	1	0	17	0	0.08	2.5×10^8	200	100	33.076
27	2	2	1	1000	2	10	8	1	0.00	4.0×10^8	0	200	35.604

Table 6 Regression coefficients and *p* value

Source	DF	Seq SS	Adj SS	Adj MS	*F* value	*p* value
B	2	3981.09	3981.09	1990.5	51.16	0.005
A	2	67.27	67.27	33.64	0.86	0.036
C	2	8.82	8.82	4.41	0.11	0.898
D	2	84.42	84.42	42.21	1.08	0.040
E	2	31.11	31.11	15.56	0.40	0.014
F	2	58.04	58.04	29.02	0.75	0.573
G	2	44.62	44.62	22.31	0.57	0.636
H	2	33.50	33.50	16.75	0.43	0.099
I	2	41.90	41.90	20.95	0.54	0.650
J	2	21.62	21.62	10.81	0.28	0.783
K	2	6.73	6.73	3.37	0.09	0.920
L	2	21.34	21.34	10.67	0.27	0.085
Error	2	77.82	77.82	38.91		
Total	26	4478.29				

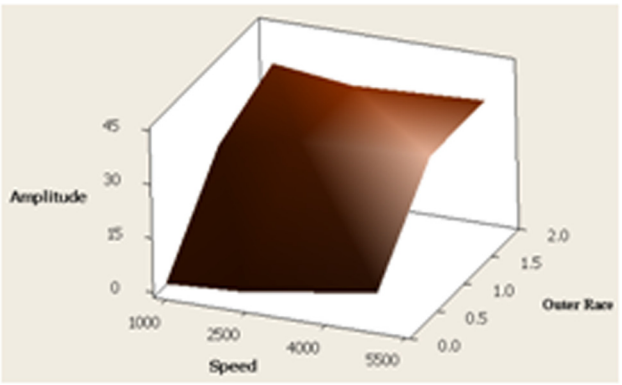

Fig. 15 Response surfaces showing interaction of amplitude with parameters *A* and *D*

signature that could not be simulated but must be taken into consideration. Only with real data is it possible to work under real environment conditions. We will show and analyze some real examples to illustrate how the theory appears in practice. First of all, variations of the bearing geometry and assembly make it impossible to precisely determine bearing characteristics frequencies. The fault severity progress can alter the bearing geometry, contributing to the increase of complexity of the diagnosis process. Operating speed and loads of the shaft greatly affect the way and the amount a machine vibrates causing bearing basic frequencies to deviate from the calculated value.

For the developed setup and the data from the ANN process carried out on the setup, a DA of the process was developed. Considering the different parameters having an effect on the amplitude of vibrations, an equation was developed from regression analysis with origin software. To validate the model, further experiments were carried out and the observed values of experiment were plotted with the values estimated from the equation obtained from regression analysis. The relative curve we get through experimental and theoretical are almost showing the same behavior as shown in Fig. 18. This model can be utilized for an ANN process, where the amplitude and frequencies obtained are a function of the listed parameters. It is clear from the results that the neural network model is better than the regression model because its results are quite nearer to actual results, whereas the regression model is performing better only if the R^2 value is high, near to 100%. ANN modeling consumes less time with a higher degree of accuracy. Hence, it can be concluded that ANN is highly effective for predicting defects and vibration amplitudes.

Overall, the defect on the inner race causes quite a chaotic system response characterized by a lot of frequency spikes in the abroad band and significantly increased displacement and force response magnitudes. This is consistent with observations obtained from the study of the experimental data based models, which reveal that the surface defects on the moving race (inner race) tends to cause more complicated dynamic behaviors with

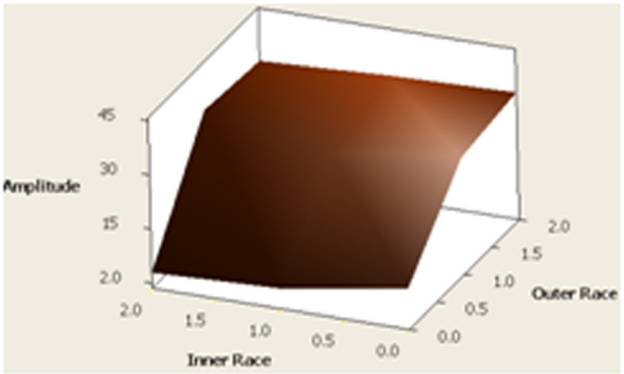

Fig. 16 Response surfaces showing interaction of amplitude with parameters *A* and *B*

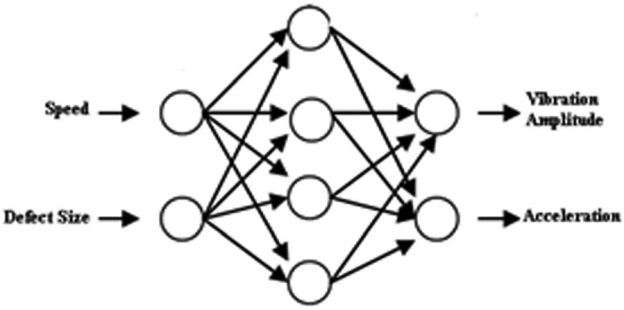

Fig. 17 Structure of the neural network

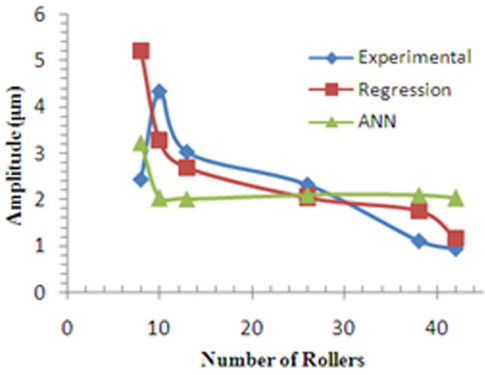

Fig. 18 Number of rollers versus amplitude

the enriched resonant frequency pool. The distinct characteristic frequencies are the cage passing frequency with respect to the inner race, observed in the horizontal and vertical displacement responses, respectively. These phenomena can potentially be applied to distinguish the moving race defect from the moving race surface waviness.

The size of the point defect is similar as the inner race point defect in Fig. 3. For vertical displacement and force, the point defect on the outer race increases the response magnitude by one order without significantly altering the amplitude frequency pattern. And the most dominant frequencies are the roller passing frequency and its super harmonics. To investigate the influence of the defect on the roller surface, it is assumed that we have a defect on the roller. As shown by Eq. (21), the defect on the roller illustrates more dramatic impacts on the axial displacement, while only showing effects on the vertical and horizontal displacement. For the horizontal displacement, the shaft frequency disappears as a dominant frequency. Similar as the defects on the inner and outer races, the defect on the roller surfaces causes increased vertical force responses in a broad band. The vibration signature of Fig. 4 shows the existence of multiples of the rolling bearing cage characteristic frequency indicating that the bearing condition is critical.

7 Conclusions

In the present investigation, a numerical model of a high-speed rotor–bearing system has been developed using DA to obtain vibration responses due to localized defects. The results have been validated under various bearing localized defect conditions with experiments performed in a sugar factory and laboratory. The present work used DOE and MVRA procedures to conduct several trials for investigating the effects of simultaneous localized defects with three levels of ID fan–rotor speeds, and analyzed the combined effects of the various localized parameters. All trials were designed to be able to consider the two-way interactions between various factors as well as main effects of individual factors. From the obtained responses, the following conclusions are drawn:

- Through model analysis, the BPT using DA or experimental data based model (EDBM) for vibration amplitude of double row spherical roller bearings are established and introduced into the vibration analysis. Considering structure stiffness, damping of the bearing, material properties, and geometrical parameters, a new state relationship between various parameters of bearings are established. On this basis, a new theory for spherical roller bearings using BPT (DA) is created.
- Vibration amplitudes significantly increase in the presence of load, defects, and speed in comparison to healthy bearings.
- Outer race radial vibration yields high amplitude of vibrations in comparison to inner race and rollers with external defects.
- Figure 17 shows the comparison between the experimental values and the predicted values by MVRA as well as the ANN model. The percentage error found in the ANN model range from −1.71% to 4.48% while the same obtained through regression equations ranges from −10.87% to 12%. It is found that the artificial neural network provides better predictions than regression analysis. ANN modeling consumes less time with a higher degree of accuracy. Hence, it can be concluded that ANN is highly effective for predicting vibration amplitude and defect frequencies of the antifriction bearings.
- The results obtained are agreeing with physical reasoning and expectations. The dependence of the amplitude of vibration on these parameters is tallying with the function of nondimensional parameters given in Eq. (19).

Acknowledgment

The authors gratefully acknowledge the help and cooperation of Dr. P. Bangarubabu, Department of Mechanical Engineering, National Institute of Technology (NIT), Warangal, India, in carrying out the real experiments. And the authors also wish to thank Sugar Factory bearing division, for support of this work and permission to publish.

Nomenclature

BPT = Buckingham's π theorem
DA = dimensional analysis (experimental data based model)
ID = induced draft
MVRA = multivariable regression analysis

Technical Specifications (Fig. 6)

anvil wrap angle = 160 deg
effective width = 1700 mm
number of hammers = 102
swing diameter = 2000 mm
weight of hammer = 20 kg

Operating Parameter

lifting of equipment = minimum 15 ton capacity crane required for loading, unloading, and erection of ID fan

References

[1] Patel, V. N., Tandon, N., and Pandey, R. K., 2010, "A Dynamic Model for Vibration Studies of Deep Groove Ball Bearings Considering Single and Multiple Defects in Races," ASME J. Tribol., **132**, p. 041101.

[2] Harsha, S. P., and Kankar, P. K., 2004, "Stability Analysis of a Rotor Bearing System Due to Surface Waviness and Number of Balls," Int. J. Mech. Sci., **46**, pp. 1057–1081.

[3] Bachschmid, N., Pennacchi, P., and Vania, A., 2002, "Identification of Multiple Faults in Rotor Systems," J. Sound Vib., **254**(2), pp. 327–366.

[4] Rahnejat, H., and Gohar, R., 1985, "The Vibrations of Radial Ball Bearings," Proc. Inst. Mech. Eng. Part C, **199**(C3), pp. 181–193.

[5] Choy, F. K., Zhou, J., Braun, M. J., and Wang, L., 2005, "Vibration Monitoring and Damage Quantification of Faulty Ball Bearings," ASME J. Tribol., **127**, pp. 776–783.

[6] Tomovic, R., Miltenovic, V., Banic, M., and Miltenovic, A., 2010, "Vibration Response of Rigid Rotor in Unloaded Rolling Element Bearing," Int. J. Mech. Sci., **52**, pp. 1176–1185.

[7] Patil, M. S., Mathew, J., Rajendrakumar, P. K., and Desai S., 2010, "A Theoretical Model to Predict the Effect of Localized Defect on Vibrations Associated With Ball Bearings," Int. J. Mech. Sci., **52**, pp. 1193–1201.

[8] Kankar, P. K., Sharma, S. C., and Harsha, S. P., 2011, "Fault Diagnosis of Ball Bearings Using Machine Learning Methods," Expert Syst. Appl., **38**(3), pp. 1876–1886.

[9] McFadden, P. D., and Smith, J. D., 1984, "Model for the Vibration Produced by a Single Point Defect in a Rolling Element Bearing," J. Sound Vib., **96**(1), pp. 69–82.

[10] McFadden, P. D., and Smith, J. D., 1985, "Model for the Vibration Produced by a Multiple Point Defect in a Rolling Element Bearing," J. Sound Vib., **98**(2), pp. 263–273.

[11] Tandan, N., Yadava, G. S., and Ramakrishna, K. M., 2007, "A Comparison of Some Condition Monitoring Techniques for the Detection of Defect in Induction Motor Ball Bearing," Mech. Syst. Signal Process., **21**, pp. 244–256.

[12] Tandan, N., and Choudhury, A., 1999, "A Review of the Vibration and Acoustic Measurement Methods for Detection of Defects in Rolling Element Bearings," Tribol. Int., **32**(8), pp. 469–480.

[13] Zeki, K., and Karagulle, H., 2006, "Vibration Analysis of Rolling Element Bearing With Various Defects Under the Action of an Unbalanced Force," Mech. Syst. Signal Process., **20**, pp. 1967–1991.

[14] Arslan, H., and Akturk, N., 2008, "An Investigation of Rolling Element Vibrations Caused by Local Defects," ASME J. Tribol., **130**(4), p. 041101.

[15] Harris, T. A., 2001, *Rolling Bearing Analysis*, 4th ed., Wiley-Interscience, New York.

[16] Desavale, R. G., Venkatachalam, R., and Chavan, S. P., 2013, "Antifriction Bearings Damage Analysis Using Experimental Data Based Models," ASME J. Tribol., **135**(4), p. 041105.

[17] Upadhyay, S. H., Harsha, S. P., and Jain, S. C., 2008, "Nonlinear Vibration Signature Analysis of High Speed Rotor Due to Defects of Rolling Element," Adv. Theor. Appl. Mech., **1**(7), pp. 301–314.

[18] Montgomery, D. C., 2007, *Design and Analysis of Experiments*, 5th ed., Wiley, Singapore, pp. 21–46.

[19] Czeslaw, T., and Kowalski, T. K., 2003, "Neural Networks Application for Induction Motor Faults Diagnosis," Math. Comput. Simul., **63**, pp. 435–448.

[20] Hoffman, A. J., and Merwe, N. T., 2002, "The Application of Neural Networks to Vibrational Diagnostics for Multiple Fault Conditions," Comput. Stand. Interfaces, **24**, pp. 139–149.

[21] Langhaar, H. L., 1951, *Dimensional Analysis and Theory of Models*, John Wiley, London, pp. 13–42.

[22] Adams, M. L., 2010, *Rotating Machinery Vibration: From Analysis to Troubleshooting*, 2nd ed., CRC Press, Boca Raton, FL.

[23] Rao, J. S., 2000, *Vibratory Condition Monitoring of Machines*, Narosa Publishing House, New Delhi, pp. 132–184.